American Mineralogist, Volume 96, pages 1568–1574, 2011

Quantum-mechanical calculations of the Raman spectra of Mg- and Fe-cordierite†

Reinhard Kaindl,* Daniel M. Többens, and Udo Haefeker

Institute of Mineralogy and Petrography, University Innsbruck, Innrain 52, A-6020 Innsbruck, Austria

Abstract

Quantum-mechanical calculations with a hybrid HF/DFT Hamiltonian (B3LYP) model yielded the Raman-active vibrational modes of the Mg- and Fe-cordierite structure. Maximum and mean deviation between experimentally derived bands and calculated modes of synthetic Mg- and natural Fe-rich cordierite are ±19 and 7 cm^{-1}. Most of the observed bands could be related to specific vibrational modes of tetrahedral and octahedral sites of the cordierite structure, although the large number of Raman-active modes (87) prevents a complete assignment. Atomic motions in cordierite are compared with those of the structurally similar mineral beryl. The calculations enable more accurate interpretation of the Raman spectra with respect to structural changes of cordierite, in particular Al-Si ordering and Mg-Fe exchange.

Keywords: Raman spectroscopy, cordierite, quantum-mechanical calculations, band assignment, Al-Si ordering, Mg-Fe exchange.

Introduction

The Mg-Fe silicate cordierite is a common natural mineral in the Earth's crust and an important synthetic component for technical applications in the fields of ceramics and microelectronics. It shows several physical and chemical properties, which have been investigated by numerous authors over 50 yr. Based on the Mg-Fe exchange with garnet, cordierite can be used as a geothermobarometer (Bhattacharya 1986). It incorporates variable amounts of volatiles like H_2O, CO_2, N_2, CO, H_2, O_2, He, Ne, Ar, CH_4, and H_2S, which makes it a potential "detector" of palaeofluid composition (Harley et al. 2002; Bul'bak and Shvedenkov 2005; Rigby et al. 2008). It substitutes substantial amounts of major, minor, and trace elements like Na, K, Mn, Li, and Be (Thompson et al. 2002; Bertoldi et al. 2004). And, finally, it is interesting from a crystal-chemical and structural point of view (e.g., Armbruster 1985; Thompson et al. 2002; Harley et al. 2002; Bertoldi et al. 2004; Yakubovich et al. 2004; Bul'bak and Shvedenkov 2005).

Cordierite is a framework silicate, containing corner-sharing tetrahedra linked into six-membered rings. It occurs in a high-temperature hexagonal structure (space group *P6*/*mcc*), where Al and Si atoms show no long-range order and a low-temperature orthorhombic form (space group *Cccm*), where complete Al-Si ordering can be attained (Armbruster and Bloss 1981; McMillan et al. 1984; Armbruster 1985; Poon et al. 1990).

Vibrational spectroscopy has been used in numerous previous investigations to examine electronic and vibrational absorption (Farrell and Newnham 1967), polymorphism (Langer and Schreyer 1969), volatile content (Vry et al. 1990; Kalt 2000; Kolesov and Geiger 2000; Yakubovich et al. 2004; Bul'bak and Shvedenkov 2005; Khomenko and Langer 2005; Kaindl et al. 2006; Kolesov 2006; Rigby et al. 2008; Weikusat et al. 2010), Al-Si ordering (McMillan et al. 1984; Poon et al. 1990), structural heterogeneity and energetics (Geiger and Grams 2003), and radiation-induced damage (Nasdala et al. 2006; Weikusat et al. 2008; Miletich et al. 2010). Although ab initio total energy studies of orientation and hydration energy of H_2O in cordierite exist (Winkler et al. 1994, 1995; Winkler 1996), to the best of our knowledge, a comprehensive study assigning experimentally observed bands to vibrational modes is lacking. We therefore present quantum-mechanical calculations of the Raman-active vibrational modes in Mg- and Fe-cordierite. We provide a comparison to experimental spectra, detailed band assignments, and some consequences for the Mg-Fe exchange and Al-Si ordering of cordierite.

Experimental methods

Synthesis of Mg- and Fe-cordierite

The starting material for the synthesis of Mg-cordierite was a homogenous glass with the composition $Mg_2Al_4Si_5O_{18}$. The oxides MgO, Al_2O_3, and SiO_2 were fired, weighed, and ground in an agate mortar. The dry mix was melted in a Carbolite HTF 1800 furnace in air in a Pt-crucible at 1700 °C for 10 min and then quenched in distilled water. Homogeneity and stoichiometry of all glassy and crystalline reaction products were checked with a JEOL JXA 8100 electron microprobe. Heat treatment of the glass allowed crystallization of cordierite. In the first step, at 800 °C and a time of 25 min, the nucleation of cordierite was activated. After 25 h at 975 °C and 24 h at 1200 °C, a disordered hexagonal cordierite was crystallized. To achieve a higher degree of Si-Al-ordering in the orthorhombic end-product, the Mg-cordierite was finally tempered at 1400 °C for 348 h. The

* Present address: Materials–Institute for Surface Technologies and Photonics, Functional Surfaces, Joanneum Research Forschungsgesellschaft mbH, Leobner Strasse 94, A-8717 Niklasdorf, Austria. E-mail: reinhard.kaindl@joanneum.at

† Open Access, thanks to the authors' funding. Article available to all readers via GSW (http://ammin.geoscienceworld.org) and the MSA web site.

so-called distortion indices of 0.243 (Miyashiro 1957) and –0.709 (Mirwald and Kirchner 1984) were determined with a STOE stadi MP high-resolution powder X-ray diffractometer system, equipped with a "Mythen" 1k detector, in bisecting transmission geometry.

The starting material for the crystallization of Fe-cordierite was a glass with the composition $Fe_2Al_4Si_5O_{18}$. The dry oxides FeO, Al_2O_3, and SiO_2 were fired, weighed, and ground in a planetary mill for 1 h. An oxide mixture with the stoichiometry $Fe_{2.3}Al_4Si_5O_{18}$ was melted in a furnace at 1700 °C for 2:30 min in a 70 µL Al_2O_3-crucible, which was placed in a covered carbon crucible. The melt was then quenched in distilled water. Because of the reducing atmosphere during the melting process, elementary iron formed. Apart from the elementary iron, which could be found as sparsely scattered small spheres, the glass was homogenous and showed the composition $Fe_2Al_4Si_5O_{18}$. For the crystallization of disordered hexagonal Fe-cordierite, the glass was tempered in a furnace at 900 °C for 21 h together with graphite-powder in a sealed gold capsule. To achieve a higher degree of Si-Al-ordering in the orthorhombic end-product, the Fe-cordierite was welded in a gold capsule and treated in a hydrothermal apparatus for 2 weeks at 700 °C and 2 kbar.

Raman spectroscopy

The unpolarized spectra of synthetic cordierite were measured on a Labram HR-800 confocal Raman-spectrometer by HORIBA, using the 532 nm excitation wavelength of a 30 mW Nd:YAG laser, through a 100× objective with a numerical aperture of 0.9. The size and power of the laser spot on the surface was approximately 1 µm and 5 mW, respectively. The confocal pinhole and entrance slit were set to 1000 and 100 µm, respectively. The scattered Raman light was dispersed by a grating with 1800 lines/mm and detected by an open-electrode CCD with 1024 × 256 pixels, each sizing 43 µm. The spectral resolution, determined by measuring the Rayleigh line, was 1.4 cm^{-1}. Background and Raman bands were fitted by the built-in spectrometer software LabSpec to first- or second-order polynomials and convoluted Gauss-Lorentz functions. Accuracy of Raman line shifts, checked by regular measurements of the emission lines of a Ne spectral calibration lamp, was on the order of 0.5 cm^{-1}.

Calculation procedures

The program CRYSTAL 06 (Dovesi et al. 2006) was used for the calculations. The vibrational modes were calculated in harmonic approximation at the Γ-point, from numerically computed second derivatives of the energy at a stationary point on the potential energy surface (Pascale et al. 2004), using 3D-periodic density functional theory and Gaussian basis sets. The B3LYP hybrid functional was used, since it proved to be much more stable than the other functionals tested in the modeling of the spin-polarized Fe-cordierite. Default settings of the program were used unless otherwise mentioned. The level of numerical accuracy was increased over the default settings of the software for the tolerances for coulomb and exchange sums (keyword TOLINTEG 7 7 7 7 15), and for the numerical integration of the DFT exchange-correlation contribution [using a (75974)p grid with keyword XLGRID]. A Pack-Monkhorst k net with 4 × 4 × 4 points in the Brillouin zone was used. All computations were done on a customary Intel Quad-Core PC running a Linux system.

As basis sets for silicon, aluminum, magnesium, and oxygen, respectively, an 86-311G(1) contraction (Pascale et al. 2005), an 88-311G(1) contraction (Towler et al. 1994), coefficients (Harrison unpublished results), an 8-511G(1) contraction based on the 8-511G contraction given in McCarthy and Harrison (1994), and an 8-411G(1) contraction based on the 8-411G contraction given in Towler et al. (1994) were used. For the Fe^{2+} in Fe-cordierite, an 86-4111G(41) contraction based on the 86-411G(41) set of Towler (Valerio et al. 1995) was used. For all basis sets, the exponents of the two most diffuse sp shells and of the one most diffuse d shell have been re-optimized, which resulted in a significant improvement. For all elements but Fe^{2+}, this optimization was done in the Mg-cordierite structure. The values of the optimized exponents are: sp(Fe) = 0.567, 0.248, d(Fe) = 0.278, sp(Si) = 0.344, 0.13, d(Si) = 0.677, sp(Al) = 0.438, 0.212, d(Si) = 0.582, sp(Mg) = 0.600, 0.315, d(Si) = 0.426, sp(O) = 0.466, 0.195, d(O) = 0.538. A high-spin state with a total unit-cell spin of 16, thus four unpaired d-electrons for each Fe^{2+}, was forced in the calculation of Fe-cordierite, since this choice resulted in the best geometry and lowest electronic energy.

The crystallo-chemical classification of the modes was based on a critical interpretation of the mode classification embedded in the CRYSTAL06 code (Dovesi et al. 2006). For this procedure in step 1, large relative motions of a pair of bonded atoms A and B, i.e., within van der Waals distance, were examined. In step 2, this motion was decomposed in a longitudinal component along the A-B bond, an angular one on the plane containing a third atom, and one out-of-the-plane component. Based on the relative contribution of these components the modes are tentatively classified as stretching modes (s), bending modes (b), or other (o), including modes likely to be rotational (r). Mode classification is given in Tables 1 and 2. In dubious cases, a decision was based on optical interpretation [using the JmolEdit applet and vibrational modes on a web page[1] using Jmol. Details and animations of all modes in the cordierite end-member and the isotopic shifts in the substituted Fe-Mg structures can be viewed by the CRYSTAL output files, provided as supplementary material[2], and web-based software [J-ICE: A Jmol Interface for Crystallographic and Electronic properties (http://j-ice.sourceforge.net)] or on a web page[1] using Jmol.

[1] http://www.theochem.unito.it/crystal_tuto/mssc2008_cd/jmoledit/index.html

[2] Deposit item AM-11-052, Supplementary material. Deposit items are available two ways: For a paper copy contact the Business Office of the Mineralogical Society of America (see inside front cover of recent issue) for price information. For an electronic copy visit the MSA web site at http://www.minsocam.org, go to the *American Mineralogist* Contents, find the table of contents for the specific volume/issue wanted, and then click on the deposit link there.

TABLE 1. Experimentally determined wavenumber (cm^{-1}) of Raman bands in synthetic Mg-cordierite, calculated modes and deviations to measured spectral bands, and mode classifications

Exp.	Calc.	Δ	Classification	Exp.	Calc.	Δ	Classification	Exp.	Calc.	Δ	Classification	Exp.	Calc.	Δ	Classification
108	99	9	$r(T_1)6)$		266		$b(T_2)6,T_1)6)$		466		$b(T_1)6),o(T_2)1,T_2)3)$	775	770	5	$s(T_1)1)b(T_1)6,M)$
116	119	–3	$o(T_1)6)$		272		b(M)	476	479	–3	$o(T_1)6)$	811	817	–5	$s(T_1)1),b(T_1)6)$
122	128	–6	$b(T_2)1,T_2)3)$	282	288	–6	$b(T_1)1,M)$	491	490	1	$b(M,T_2)6)$	901	902	–1	$s(T_2)1,T_2)3)$
129	133	–4	$b(M,T_1)1),o(T_1)6)$	295	297	–2	$b(T_1)1,T_2)3)$		495		$s(M),o(T_1)6)$		906		$s(T_2)1,T_2)3)$
	133		$b(T_2)6,T_1)6)$		298		$b(T_2)1,T_2)3,T_2)6)$		497		$b(T_2)6,M)$		909		$s(T_1)6)$
140	134	6	$b(M,T_1)6),o(T_1)1)$		298		$b(T_1)1,T_2)3),o(M,T_1)6)$		500		$s(M),o(T_1)6)$	922	931	–9	$s(T_1)1,T_2)1,T_2)3)$
158	162	–4	$o(T_1)1),b(T_1)6)$		303		b(M)	556	556	0	$s(T_2)6,M),b(T_1)6,T_2)6)$	952	964	–12	$s(T_2)1,T_1)6)$
	162		$b(T_2)1,T_2)3)$	307	306	1	$o(T_1)1)$		562		$s(T_2)6,M),b(T_2)6,T_2)1,T_2)3)$	974	978	–4	$s(T_2)1,T_2)3)$
172	170	2	$b(T_2)6,T_1)6)$	322	315	7	$b(T_2)1,T_2)3,T_2)6)$	571	574	–3	$s(M),b(T_2)1,T_2)3,T_2)6)$		988		$s(T_2)6)$
	177		$b(M,T_1)1)$		330		$b(T_1)6,T_2)1,T_2)3)$	580	586	–6	s(M)		988		$s(T_1)6,T_2)1,T_2)3)$
	184		$o(M,T_1)1,T_1)6)$	329	330	–1	$b(M),o(T_1)1,T_1)6)$		603		$s(T_2)6)$		989		$s(T_2)1,T_2)3)$
	189		$o(T_2)6)$		342		$b(M,T_2)6)$	628	631	–3	$s(T_1)1)$	1013	1015	–2	$s(T_2)1,T_2)3)$
	190		o(M)		359	4	o(M)		636		$s(M),b(T_2)3,T_2)1T_1)6)$		1015		$s(T_1)6,T_2)1,T_2)3)$
	203		$o(T_1)6)$	363	363	3	b(M)		664		$s(T_1)1)$		1036		$s(T_1)6,T_2)1,T_2)3)$
209	213	–4	$o(T_1)1)$	366	370	–3	b(M)	673	672	1	$s(T_1)1)$	1092			
	221		$b(M),o(T_1)1)$	367	378	11	$s(M,T_1)1,T_1)6),b(M,T_1)1)$	694	688	6	$s(T_2)6,T_1)6)$	1113	1129	–16	$s(T_2)1,T_2)3)$
241	244	–3	$b(M),o(T_1)1)$	386	386	0	$b(T_1)1,M)$	714	705	9	$b(T_2)6,M),s(T_2)6)$		1131		$s(T_2)1,T_2)3)$
	245		$b(T_2)6,T_2)1)$		398		$s(M),o(T_1)1)$	726	728	–2	$s(T_2)6),b(T_2)1,T_2)3),$	1164	1176	–12	$s(T_2)1,T_2)3)$
	246		$b(T_2)6,T_2)3)$	430	424	6	$b(T_2)6)$		737		$b(T_2)3,M)$	1190	1177	13	$s(T_2)1,T_2)3)$
	250		$b(T_2)6,T_2)1)$		435		$b(T_2)6,T_2)1,T_2)3,T_1)6)$	741	742	–1	$b(T_2)1,T_2)3,M)$		1210		$s(T_2)1,T_2)3)$
256	260	–4	$b(M),o(T_1)1)$	456	461	–5	$o(T_2)1,T_2)3)$	755	756	–1	$b(T_1)1),s(T_1)1,T_2)1,T_2)3)$	1221	1213	8	$s(T_2)1,T_2)3)$
261	266	–5	b(M)		462		$b(T_2)1,T_2)3,T_2)6)$		760		$b(T_2)1,T_2)3)$				

Note: Exp. = experimental; Calc. = calculated; Δ = difference exp. – calc.; s = stretching; b = bending; o = other; r = rotational; standard deviation between measured and calculated modes is 6 cm^{-1}.

TABLE 2. Experimentally determined wavenumber (cm^{-1}) of Raman bands in synthetic Fe-cordierite, calculated modes and deviations to measured bands, and mode classifications

Exp.	Calc.	Δ	Classification	Exp.	Calc.	Δ	Classification	Exp.	Calc.	Δ	Classification	Exp.	Calc.	Δ	Classification
108	104	4	b(M)	260	258	2	b($T_2$6,$T_1$6)	476	476	0	o($T_2$1,$T_2$3)	775	756	19	b($T_2$1,$T_2$3)
112	105	7	o($T_1$1,M)		266		b($T_2$1)	482	489	–7	o($T_1$6)		812		s($T_1$1),b($T_1$6)
116	118	–2	b($T_1$1,M)		278		o($T_1$1)		494		b($T_2$6,$T_1$1)				
124	133	–9	b($T_2$1,$T_2$3)	293	292	1	b(M)		498		b(M,$T_2$6)		903		s($T_2$1,$T_2$3)
	134		b(M)		296		b($T_1$1,$T_2$3)		502		o($T_1$6,$T_2$1,$T_2$3)	909	908	1	s($T_2$1,$T_2$3)
140	136	4	b(M,$T_1$6),o($T_1$1,$T_2$6)		298		b($T_1$1,M,$T_2$6)		513		o($T_2$1,$T_2$3)	924	935	–11	s($T_1$6)
148	144	4	o(M,$T_1$1)		298		b($T_2$1,$T_2$3)	552	564	–12	s($T_2$6,M),b($T_1$6,$T_2$6)		938		s($T_1$1,$T_2$1,$T_2$3)
154	154	0	b(M),o($T_1$1,$T_2$6,$T_2$1,$T_1$6)	308	307	1	b(M)	557	567	–10	s($T_2$6,M,$T_2$1,$T_2$3)	961	973	–12	s($T_2$1,$T_2$3)
	158		b(M)		313		b($T_2$6,$T_2$1,$T_2$3)	573	582	–9	s(M),o($T_1$6),b($T_2$1,$T_2$3)	967	978	–11	s($T_1$6)
	163		o(M,$T_2$1,$T_2$3),b(M,),s(M)	322	317	5	b($T_1$1,M),o($T_2$6)	594	601	–7	s($T_2$6)		983		s($T_2$1,$T_2$3)
	167		b($T_2$1,$T_2$3)	332	330	2	b(M)		603		s(M),b($T_1$6,$T_2$1,$T_2$6)		986		s($T_2$1,$T_2$3)
171	172	–1	b($T_2$6,$T_2$1,$T_2$3)		336		b($T_2$1,$T_2$3)		615		s($T_1$1)		994		s($T_2$6)
194	202	–7	o(M,$T_1$1,$T_2$6)		339		s(M,$T_2$6),o($T_1$1)		633		b($T_2$6,$T_1$6)	1009	1021	–12	s($T_1$6)
	206		o($T_1$1)		344		b($T_1$1,$T_2$1,$T_1$6,$T_2$3)	665	666	–1	b($T_1$1)		1041		s($T_1$6)
	209		o($T_1$6,$T_2$1,$T_2$3)		346		s($T_1$1,M),o($T_1$6)		675		b($T_2$6,$T_2$1,$T_2$3)		1063		s($T_2$1,$T_2$3)
	212		s($T_2$6,M),b($T_2$6,M)	364	352	12	b(M,$T_2$1,$T_2$3)		684		s($T_1$1)	1091			
	214		o($T_1$1,$T_2$3)		381		b(M,$T_1$1,$T_1$6)	707	700	7	b($T_2$6,M),s($T_2$6)	1104	1122	–18	s($T_2$1,$T_2$3)
	226		s($T_2$6,M),b($T_2$1,$T_1$1)		403		o($T_2$6)	724	715	9	s($T_2$6)		1123		s($T_2$1,$T_2$3)
234	229	5	b($T_2$6,M,$T_2$1,$T_2$3)	419	427	–8	b($T_2$6)		733		b($T_2$3)	1156	1171	–15	s($T_2$1,$T_2$3)
239	239	0	o($T_1$6)	450	437	13	b($T_2$6,$T_2$1,$T_2$3, $T_1$6)		744		b($T_1$1,$T_2$1,$T_2$3)	1176	1177	–1	s($T_2$1,$T_2$3)
	248		o(M)	459	464	–5	b($T_2$1,$T_2$3)		744		b($T_2$1,$T_2$3,$T_2$6)		1198		s($T_2$1,$T_2$3)
256	258	–2	b(M)	468	473	–5	b($T_1$6)		751		b($T_1$6,M)		1203		s($T_2$1,$T_2$3)

Note: Abbreviations same as in Table 1; standard deviation between measured and calculated modes is 8 cm^{-1}.

RESULTS AND DISCUSSION

Structure of cordierite

The silicate cordierite with the simplified formula $(Mg,Fe)_2Al_4Si_5O_{18}$ is comprised of a tetrahedral framework structure. A crystal-chemical formula of low-cordierite in the space group *Cccm* can be written as follows (Cohen et al. 1977; Armbruster 1986; Bertoldi et al. 2004):

$$(M)_2(T_23)_2(T_21)_2(T_26)_2(T_16)(T_11)_2O_{18}, (Ch0,Ch¼) \quad (1)$$

where M represents an octahedrally coordinated Mg^{2+}, Fe^{2+}, or Mn^{2+} ion, T represents several tetrahedral positions, and Ch represents channel sites. The T_2 tetrahedra build six-membered rings, whereas the T_1 tetrahedra cross-link these units to form a framework structure. Silicon occupies the T_23, T_21, and T_16 sites, Al the remaining two T_11 and T_26 sites. The six-membered rings are stacked parallel to the *c*-axis, forming endless channels. The channel sites Ch0 and Ch¼ can incorporate additional ions such as Na^+ and K^+, balancing charge deficiencies, or volatiles such as H_2O and CO_2. The occupancy of the Ch sites was not considered in this study, as well as the effects of Mn^{2+} occupancy on the M site. The terms used in the formula given above are used in the following discussion.

Symmetry adaption of vibrational modes

In total, 174 vibrational modes were derived from group-theoretical calculations within the CRYSTAL 06 program suite for a cordierite structure with space group *Cccm*:

$$\Gamma_{vib} = 23\,A_g + 25\,B_{1g} + 19\,B_{2g} + 20\,B_{3g} + 17\,A_u + 19\,B_{1u} + 25\,B_{2u} + 26\,B_{3u}. \quad (2)$$

One B_{1u}, B_{2u}, and B_{3u} mode each corresponds to pure translations of the structure; 87 *g*-modes are Raman-active; of the *u*-modes 67 are IR-active. The A_u-modes are inactive (silent) modes, and were therefore not considered, since they are experimentally inaccessible.

RAMAN BANDS AND VIBRATIONAL MODES

In the following discussion, the most important Raman bands of the cordierite spectra, their assignments and relations with structural features of cordierite are considered.

Mg-cordierite

The experimentally derived Raman spectrum of Mg-cordierite is displayed in Figure 1. The uppermost vertical bars in the figure represent the wavenumber derived by band fitting, and the lower row of bars represent the wavenumber of modes calculated with the B3LYP model. Maximum and mean deviation between experimentally derived bands and calculated modes was 16 and 5 cm^{-1}, respectively (Table 1). The quality of the calculations allowed assignment of most of the high- and medium-intensity bands to specific vibrational modes. However, assignments of some weaker bands, especially in the range below 500 cm^{-1}, remained questionable. Generally, the uncertainty of the assignment is due to the proximity of multiple modes of different symmetry, but involving the same atoms and structural building units.

The Raman spectrum of Mg-cordierite is characterized by several spectral ranges, alternating with more or less pronounced, gaps. Bands in the range 900–1250 cm^{-1} are prevailing stretching vibrations of the tetrahedral sites. The band at 1190 cm^{-1} results from two A_g and B_{1g} stretching modes, which could not be resolved by the spectrometer. The two T_21 and T_23 tetrahedra stretch in counter-tact, their common oxygen moves approximately in the direction of the *a*-axis. One sharp band at 1092 cm^{-1} is also observed at the same wavenumber in the spectrum of Fe-cordierite, suggesting contamination during the synthesis. The strongest band in this range and crystal orientation was detected at 974 cm^{-1}. This band is caused by stretching of the "ring-tetrahedra" T_21, as well as the T_16 tetrahedron, which connects two M sites. The first vibrational mode involving bending

vibrations is observed after a spectral "gap" at 811 cm^{-1} and is related to Si-O tetrahedra of the $T_1$6 site, accompanied by stretching of Al-O tetrahedra of the $T_1$1 site. The next intense band at lower wavenumber at 673 cm^{-1} is again caused by stretching of the $T_1$1 Al-tetrahedra, interconnecting two M sites.

The intense, split bands between 530–600 cm^{-1} can be deconvoluted into three components at 556, 571, and 580 cm^{-1}, which are related to bending vibrations of the $T_2$6, $T_2$1, and $T_2$3 units and simultaneous stretching of the M and $T_2$6 sites. Bands below 380 cm^{-1} can be assigned to bending modes affecting mainly the T and M sites, accompanied by vibrations, which are neither dominantly stretching nor bending modes (named "other" in Table 1). Bands of medium intensity at 430 and 367 cm^{-1} result from bending of the $T_2$6 and the M site, respectively, whereas the bands at 295, 256, and 241 cm^{-1} result from bending modes of both Si- and Al-tetrahedral and M octahedral sites.

The band at 158 cm^{-1} probably involves bending of $T_2$1 and $T_2$3 "ring sites" and $T_1$1 and $T_1$6 sites interconnecting the M sites. Bands from 122 cm^{-1} down to the lower limit of the measurement range (~100 cm^{-1}) result from modes deforming and rotating mainly the $T_1$6 site.

Fe-cordierite

The maximum and mean deviation between experimentally derived bands and calculated modes here is slightly higher, namely 19 and 7 cm^{-1} (Fig. 2, Table 2). The general assignment of observed bands to vibrational modes is very similar to Mg-cordierite. Bands in the range 900–1200 cm^{-1} are stretching vibrations of the tetrahedral sites, above 1060 cm^{-1} exclusively of the $T_2$1-$T_2$3 double-tetrahedra sites, which are interconnected by common oxygen. The strong band at 1176 cm^{-1} is such a stretching mode, whereas the band at 967 cm^{-1} involves stretching of the $T_1$6 Al-containing site as well. The spectral gap of Fe-cordierite from 900 to below 800 cm^{-1} is slightly wider; the first low-intensity band after the gap involves bending of the $T_1$6 site and stretching of the $T_1$1 site.

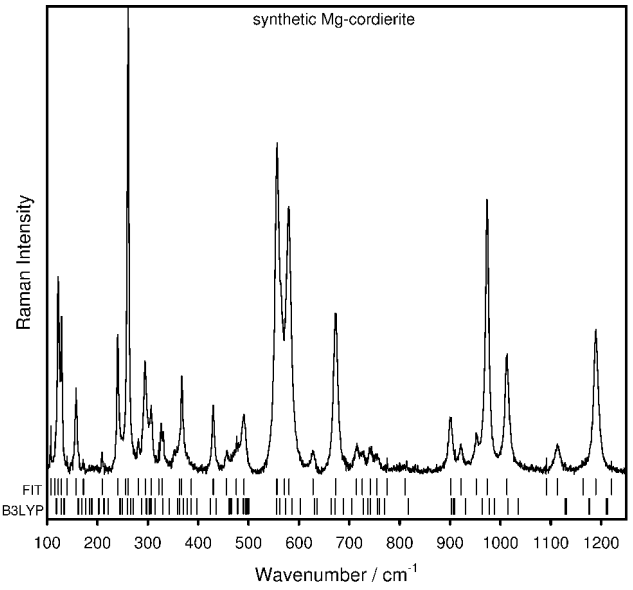

FIGURE 1. Unpolarized Raman spectrum of a synthetic Mg-cordierite single crystal in the range 100–1250 cm^{-1}. Vertical bars mark wavenumbers of experimentally determined bands (top) and modes calculated by B3LYP functionals (bottom).

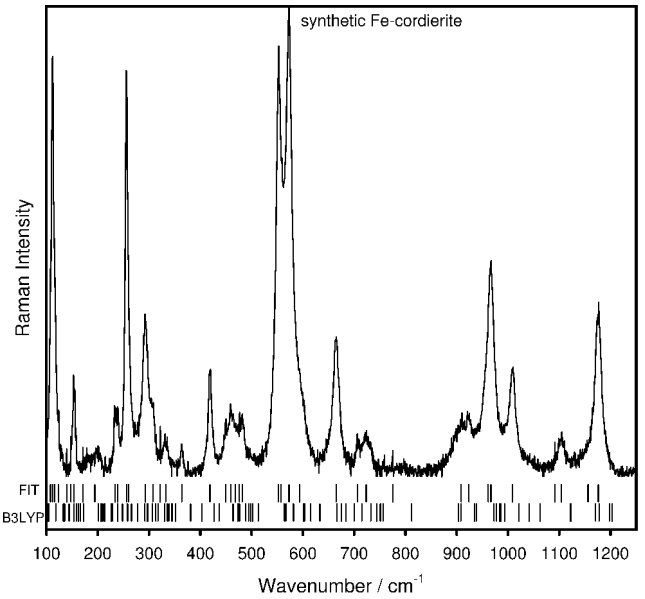

FIGURE 2. Unpolarized Raman spectrum of a synthetic Fe-cordierite single crystal in the range 100–1200 cm^{-1}. Vertical bars mark wavenumbers of experimentally determined bands (top) and modes calculated by the B3LYP functional (bottom).

The next medium intensity band at 665 cm^{-1} can be assigned to bending of the $T_1$1 site as well, although there are some weaker bands in the high wavenumber flank of this band, which involves the $T_2$6, $T_2$1, and $T_2$3 sites. The most intense triplet at 552, 557, and 573 cm^{-1} is related to very complex bending and stretching modes and not clearly classifiable movements of the tetrahedral and octahedral sites. A weak band in the high wavenumber flank at 594 cm^{-1} results from stretching vibration of the $T_1$1 site.

Below 500 cm^{-1} several bands of low to medium intensity at 482, 459, 419, 364, and 308 cm^{-1} are observed. Due to the large number of calculated modes in this range assignments are somewhat arbitrary. The band at 482 cm^{-1} probably results from a group of bending and other modes, involving, more or less, all crystallographic sites in the cordierite structure. The weak band at 459 cm^{-1} is a bending mode of the $T_2$1 and $T_2$3 sites. The same can be said for the band at 419 cm^{-1}, but also involves the $T_2$6 site. The "solitary" band at 364 cm^{-1} can be clearly assigned to bending of the "outer rim" sites $T_1$6, M, and $T_1$1. The double bands at 308 and 293 cm^{-1} are difficult to assign, as the calculated bending modes in this range involve all structural units.

Below 300 cm^{-1} two bands with strong and two bands with medium intensity are observed. The strong band at 256 cm^{-1} is probably dominated by bending modes of the M site, accompanied by bending of the $T_1$6 and $T_2$6 sites. Bending of the M site is also important for the medium intensity bands around 239 and at 154 cm^{-1}, but all tetrahedral sites contribute to this band. The strong band at 112 cm^{-1} clearly results from bending and other motion of the $T_1$1 and M sites.

Comparison beryl-cordierite

For the structurally comparable beryl ($Al_4Be_6Si_{12}O_{36}$) a quantum-mechanical calculation of the Raman (and IR) spectrum is available (Prencipe et al. 2006). Similar to cordierite, the structure of beryl consists of sixfold rings of Si tetrahedra stacked along [001]. The rings form channels, which can host water molecules and alkali cations, and are interconnected by Be tetrahedra and Al octahedra. Prencipe et al. (2006) calculated isotopic substitution of species in the unit cell and provided graphical animations of the atomic motion involved in each vibrational mode.

The structural similarity of beryl and cordierite is reflected in the atomic motions as well. For example, Prencipe et al. (2006) described anti-phase rotations around [001] of beryl Si_6O_{18} rings at 272 cm^{-1}. Similar, but more complex motions can be seen for the calculated modes at 266 cm^{-1} in both Fe- and Mg-cordierite (which do not occur in the experimental spectra). The breathing mode at 324 cm^{-1} in beryl is found at 315 and 336 cm^{-1} in Mg- and Fe-cordierite, respectively. The beryl breathing mode resulting from bending of Si, Al, and Be polyhedra at 395 cm^{-1} has its counterpart in two modes at 370 (Mg-) and 352 cm^{-1} (Fe-cordierite). The O2-Be-O2 and O2-Al-O2 bending mode at 630 cm^{-1} in beryl is calculated at a lower wavenumber (586 cm^{-1} = Mg, 582 cm^{-1} = Fe) in cordierite and the ring rotation is much weaker. The Si-O2 stretching mode coupled with O2-Al-O2 and O2-Be-O2 angles deformations at 1065 cm^{-1} corresponds to 1015 and 986 cm^{-1} in Mg- and Fe-cordierite, respectively. The asymmetric Si-O stretching mode at 1132 cm^{-1}, confined to the XY plane in beryl, is found at 1129 and 1122 cm^{-1} in Mg- and Fe-cordierite, respectively. To summarize, atomic motions of modes in beryl and cordierite are very similar but are more complex in the latter. With the exception of one breathing mode at 324 cm^{-1}, wavenumbers of modes with comparable motions are highest in beryl, intermediate in Mg-, and lowest in Fe-cordierite.

Mg-Fe exchange

Shifts of vibrational bands as a function of composition were already used for semi-quantitative chemical analysis of mineral solid solutions as, for example, for the binary and ternary pyroxene group and the garnet series (e.g., Geiger and Grams 2003; Smith 2005; Stalder et al. 2009). Geiger and Grams (2003) investigated 22 natural Mg-Fe cordierite powders by Fourier transform infrared (FTIR) spectroscopy and obtained a large number of bands between 50 and 1300 cm^{-1}. By plotting wavenumber changes as a function of composition they found a general shift of modes to lower wavenumber with increasing X_{Fe}, but also some modes with slight shifts to higher wavenumber.

In Figure 3, the deviations of experimentally derived bands of synthetic Mg-cordierite are plotted against the most likely corresponding band in Fe-cordierite. Due to the fact that we lack synthetic Mg-Fe-cordierite solid solutions with intermediate compositions, identification of corresponding bands in the end-members is difficult and somewhat arbitrary. However, almost all bands shift, more or less, toward lower wavenumber in the Fe-cordierite end-member, which is generally expected for substitutions of a lighter Mg than for the heavier Fe atom. The few bands of Fe-cordierite, which shift significantly toward higher wavenumber, are of comparable low intensity (332 cm^{-1}), very broad (909 cm^{-1}), or a flank on more intense bands (961 cm^{-1}). The strongest negative shifts of Mg-cordierite bands are observed at 1190 and 1113 cm^{-1} ($T_2$1 and $T_2$3 stretching modes), 628 cm^{-1} ($T_1$1 stretching), 571 cm^{-1} ($T_2$6 and M stretching; $T_2$6, $T_2$1, and $T_2$3 bending), 491 cm^{-1} (M and $T_2$6 bending), 476 cm^{-1} ($T_1$6 other), 430 cm^{-1} ($T_2$6 bending), and 256 cm^{-1} (M bending; $T_1$1 other). For chemical analysis these bands should be the most favorable. Furthermore, band assignments to vibrational modes show that wavenumber shifts caused by substitutions like Mg^{2+} = Fe^{2+} not only affect Si-O vibrations within or between the

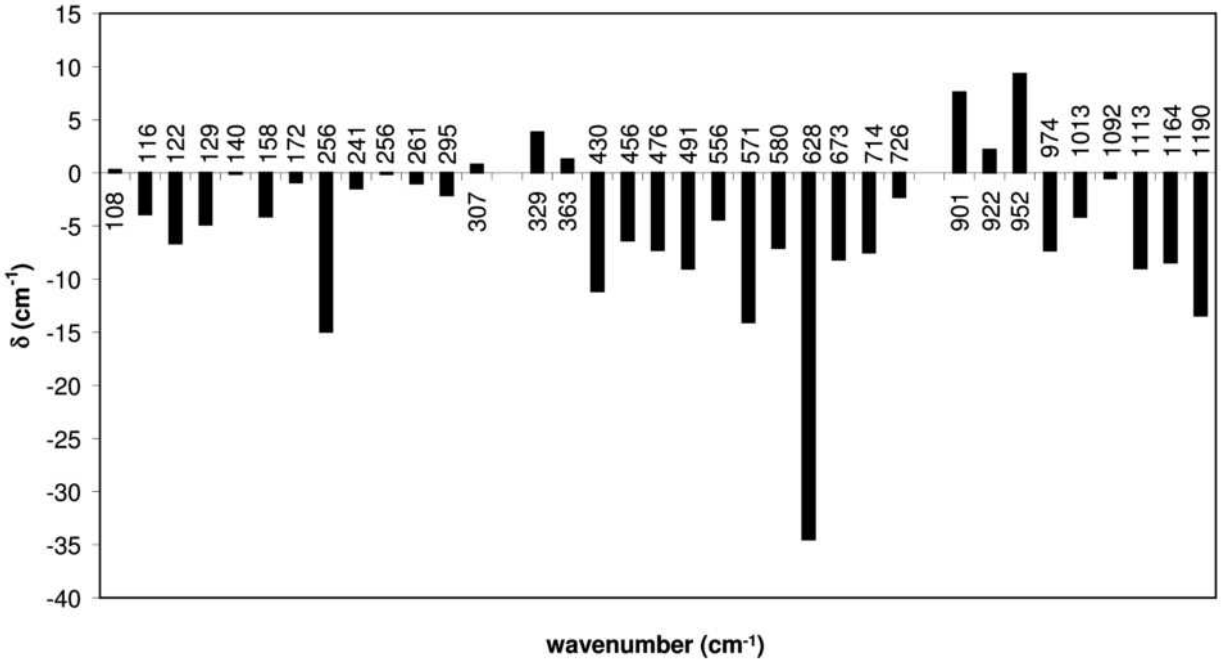

FIGURE 3. Deviations of experimentally determined bands between synthetic Mg- and Fe-cordierite crystals. The numbers give wavenumber of modes in Mg-cordierite, plotted against the deviation δ of the corresponding mode in Fe-cordierite.

tetrahedral sites (Smith 2005) but, in the case of cordierite, also directly on the mixing site, i.e., the M site.

To clarify the correspondence between the spectra of Mg- and Fe-cordierite, isotopic Fe-Mg substitutions were calculated. By substituting the Mg atomic masses with Fe masses on the force-constant matrix obtained quantum-mechanically for the Mg compound and vice versa, the effects of an isotopic substitution experiment can be emulated. By comparing the results from the different calculations, the pure mass effects on the frequencies can be isolated, as well as the pure effects of bonding. Interestingly, there seems to be two mode groups, one controlled by the mass differences between Mg and Fe and the other by the force constant, i.e., the bonding. From this analysis, it is obvious that modes at 520 cm^{-1} and above are not significantly influenced by the mass difference between Mg and Fe, but are subject to shifts either to higher or to lower frequencies caused by force constant changes alone. In contrast, for modes below this threshold, the influence of the chemical bonding is almost exclusively a small shift toward higher frequencies in the Fe compound, which for many modes is overcompensated by a strong mass effect shift toward lower frequencies.

Al-Si ordering of Mg-cordierite

In the hexagonal phase of Mg-cordierite, the Al and Si atoms have no long-range order, whereas within the orthorhombic low-temperature structure, complete Al-Si ordering can be attained (Poon et al. 1990). Natural cordierites are orthorhombic and appear to have fully ordered Al-Si distribution. More or less disordered, metastable hexagonal Mg-cordierite can be produced by different annealing times of glasses of appropriate composition, followed by rapid quenching (Putnis 1980). McMillan et al. (1984) have studied the Raman spectra with increasing annealing times and observed splitting of peaks and sharpening of lines. Poon et al. (1990) obtained quantitative results, relating mode splitting and linewidths to the local behavior of order parameters.

The symmetry change from hexagonal to orthorhombic Mg-cordierite is clearly seen in the Raman spectrum by splitting of the strongest band at 566 cm^{-1} into three components centered at ~556, 571, and 580 cm^{-1}. Our calculations show that four modes contribute to these bands. The band at 580 cm^{-1} corresponds to a stretching vibration of the M site. The band at 556 cm^{-1} is composed of two modes, dominantly stretching vibrations of the M and $T_2$6 sites and complex bending vibrations of Si and Al tetrahedral sites. The central band at 571 cm^{-1} can be assigned to stretching of the M site and bending of tetrahedral sites. Interestingly, the $T_1$1 site does not contribute. Poon et al. (1990) argued that the band at 566 cm^{-1} of hexagonal cordierite is a Si-O-Si bending mode. According to our results, in addition to the tetrahedral Si-containing sites, both Al- and M sites in orthorhombic Mg-cordierite are also involved. Another band at 672 cm^{-1} does not split on the appearance of local orthorhombic symmetry, but increases in intensity and sharpens with increasing short-range order. Our calculations indicated that this band exclusively results from stretching vibrations of the Al-containing $T_1$1 site.

The disorder-order band splitting and sharpening was attributed by Poon et al. (1990) to local distortions of scattering units to a varying degree. This can be specified now to tetrahedral and octahedral sites as presented above. It is expected that our calculations will enable more accurate and comprehensible interpretations of the Raman spectra of Mg- and Fe-cordierite in the future.

ACKNOWLEDGMENTS

Jürgen Konzett from the Institute of Mineralogy and Petrology, University Innsbruck, is acknowledged for the help with cordierite synthesis. This work was supported by the Austrian Science Fund (FWF): [P22013-N21].

REFERENCES CITED

Armbruster, T. (1985) Crystal structure refinement, Si, Al-ordering, and twinning in "Pseudo-hexagonal" Mg-cordierite. Neues Jahrbuch für Mineralogie Monatshefte, 255–267.

——— (1986) Role of Na in the structure of low-cordierite: a single-crystal X-ray study. American Mineralogist, 71, 746–757.

Armbruster, T. and Bloss, F.D. (1981) Mg-Cordierite: Si/Al ordering, optical properties, and distortion. Contributions to Mineralogy and Petrology, 77, 332–336.

Bertoldi, C., Proyer, A., Garbe-Schönberg, D., Behrens, H., and Dachs, E. (2004) Comprehensive chemical analyses of natural cordierites: implications for exchange mechanisms. Lithos, 78, 389–409.

Bhattacharya, A. (1986) Some geobarometers involving cordierite in the FeO-Al_2O_3-SiO_2 (±H_2O) system: refinements, thermodynamic calibration, and applicability in granulite-facies rocks. Contributions to Mineralogy and Petrology, 94, 387–394.

Bul'bak, T.A. and Shvedenkov, G.Y. (2005) Experimental study on incorporation of C-H-O-N fluid components in Mg-cordierite. European Journal of Mineralogy, 17, 829–838.

Cohen, J.P., Ross, F.K., and Gibbs, G.V. (1977) An X-ray and neutron diffraction study of hydrous low cordierite. American Mineralogist, 62, 67–78.

Dovesi, R., Saunders, V.R., Roetti, R., Orlando, R., Zicovich-Wilson, C.M., Pascale, F., Civalleri, B., Doll, K., Harrison, N.M., Bush, I.J., D'Arco, P., and Llunell, M. (2006) CRYSTAL06 User's Manual. University of Torino, Italy.

Farrell, E.F. and Newnham, R.E. (1967) Electronic and vibrational absorption spectra in cordierite. American Mineralogist, 52, 380–388.

Geiger, C.A. and Grams, M. (2003) Cordierite IV: structural heterogeneity and energetics of Mg–Fe solid solutions. Contributions to Mineralogy and Petrology, 145, 752–764.

Harley, S.L., Thompson, P., Hensen, B.J., and Buick, I.S. (2002) Cordierite as a sensor of fluid conditions in high-grade metamorphism and crustal anatexis. Journal of Metamorphic Geology, 20, 71–86.

Kaindl, R., Tropper, P., and Deibl, I. (2006) A semi-quantitative technique for determination of CO_2 in cordierite by Raman spectroscopy in thin sections. European Journal of Mineralogy, 18, 331–335.

Kalt, A. (2000) Cordierite channel volatiles as evidence for dehydration melting: an example from high-temperature metapelites of the Bayerische Wald (Variscan belt, Germany). European Journal of Mineralogy, 12, 987–998.

Khomenko, V.M. and Langer, K. (2005) Carbon oxides in cordierite channels: Determination of CO_2 isotopic species and CO by single crystal IR spectroscopy. American Mineralogist, 90, 1913–1917.

Kolesov, B.A. (2006) Raman spectra of single H_2O molecules isolated in cavities of crystals. Journal of Structural Chemistry, 47, 21–34.

Kolesov, B.A. and Geiger, C.A. (2000) Cordierite II: The role of CO_2 and H_2O. American Mineralogist, 85, 1265–1274.

Langer, K. and Schreyer, W. (1969) Infrared and powder X-ray diffraction studies on the polymorphism of cordierite, $Mg_2(Al_4Si_5O_{18})$. American Mineralogist, 54, 1442–1459.

McCarthy, M.I. and Harrison, N.M. (1994) Ab initio determination of the bulk properties of MgO. Physical Review B, 49, 8574–8582.

McMillan, P., Putnis, A., and Carpenter, M.A. (1984) A Raman spectroscopic study of Al-Si ordering in synthetic magnesium cordierite. Physics and Chemistry of Minerals, 10, 256–260.

Miletich, R., Diego Gatta, G., Redhammer, G.J., Burchard, M., Meyer, H.-P., Weikusat, C., Rotiroti, N., Glasmacher, U.A., Trautmann, C., and Neumann, R. (2010) Structure alterations in microporous $(Mg,Fe)_2Al_4Si_5O_{18}$ crystals induced by energetic heavy-ion irradiation. Journal of Solid State Chemistry, 183, 2372–2381.

Miyashiro, A. (1957) Cordierite-indialite relations. American Journal of Sciences, 255, 43–62.

Mirwald, P. and Kirchner, A. (1984) Zum Ordnungs-/Unordnungsverhalten von Mg-Cordierit zwischen 1400°C und dem Schmelzpunkt (1463°C). Fortschritte in der Mineralogie, 62, 157–159.

Nasdala, L., Wildner, M., Wirth, R., Groschopf, N., Pal, D.C., and Möller, A. (2006) Alpha particle haloes in chlorite and cordierite. Mineralogy and Petrology, 86, 1–27.

Pascale, F., Zicovich-Wilson, C.M., Lopez, F., Civalleri, B., Orlando, R., and

Dovesi, R. (2004) The calculation of the vibration frequencies of crystalline compounds and its implementation in the CRYSTAL code. Journal of Computational Chemistry, 25, 888–897.

Pascale, F., Zicovich-Wilson, C.M., Orlando, R., Roetti, C., Ugliengo, P., and Dovesi, R. (2005) Vibration frequencies of $Mg_3Al_2Si_3O_{12}$ pyrope. An *ab initio* study with the CRYSTAL Code. Journal of Physical Chemistry B, 109, 6146–6152.

Poon, W.C.K., Putnis, A., and Salje, E. (1990) Structural states of Mg cordierite: IV. Raman spectroscopy and local order parameter behaviour. Journal of Physics: Condensed Matter, 2, 6361–6372.

Prencipe, M., Noel, Y., Civalleri, B., Roetti, C., and Dovesi, R. (2006) Quantum-mechanical calculation of the vibrational spectrum of beryl ($Al_4Be_6Si_{12}O_{36}$) at the Γ point. Physics and Chemistry of Minerals, 33, 519–532.

Putnis, A. (1980) Order-modulated structures and the thermodynamics of cordierite reactions. Nature, 287, 128–131.

Rigby, M.J., Droop, G.T.R., and Bromiley, G.D. (2008) Variations in fluid activity across the Etive thermal aureole, Scotland: evidence from cordierite volatile contents. Journal of Metamorphic Geology, 26, 331–346.

Smith, D.C. (2005) The RAMANITA© method for non-destructive and in situ semi-quantitative chemical analysis of mineral solid-solutions by multidimensional calibration of Raman wavenumber shifts. Spectrochimica Acta Part A, 61, 2299–2314.

Stalder, R., Kronz, A., and Schmidt, B.C. (2009) Raman spectroscopy of synthetic $(Mg,Fe)SiO_3$ single crystals. An analytical tool for natural orthopyroxenes. European Journal of Mineralogy, 21, 27–32.

Thompson, P., Harley, S.L., and Carrington, D.P. (2002) Sodium and potassium in cordierite—a potential thermometer for melts? European Journal of Mineralogy, 14, 459–469.

Towler, M.D., Allan, N.L., Harrison, N.M., Saunders, V.R., Mackrodt, W.C., and Aprà, E. (1994) Ab initio study of MnO and NiO. Physical Review B, 50, 5041–5054.

Valerio, G., Catti, M., Dovesi, R., and Orlando, R. (1995) Ab initio study of antiferromagnetic rutile-type FeF_2. Physical Review B, 52, 2422–2427.

Vry, J.K., Brown, P.E., and Valley, J.W. (1990) Cordierite volatile content and the role of CO_2 in high-grade metamorphism. American Mineralogist, 75, 71–88.

Weikusat, C., Glasmacher, U.A., Miletich, R., Neumann, R., and Trautmann, C. (2008) Raman spectroscopy of heavy ion induced damage in cordierite. Nuclear Instruments and Methods in Physics Research B, 266, 2990–2993.

Weikusat, C., Miletich, R., Glasmacher, U.A., Trautmann, C., and Neumann, R. (2010) Heavy-ion irradiation on crystallographically oriented cordierite and the conversion of molecular CO_2 to CO: a Raman spectroscopic study. Physics and Chemistry of Minerals, 37, 417–424.

Winkler, B. (1996) The dynamics of H_2O in minerals. Physics and Chemistry of Minerals, 23, 310–318.

Winkler, B., Milman, V., and Payne, M.C. (1995) Ab Initio total energy studies of minerals using density functional theory and the local density approximation. Mineralogical Magazine, 59, 589–596.

Winkler, B., Milman, V., and Payne, M.C. (1994) Orientation, location, and total energy of hydration of channel H_2O in cordierite investigated by ab-initio total energy calculations. American Mineralogist, 79, 200–204.

Yakubovich, O.V., Massa, V., Pekov, I.V., Gavrilenko, P.G., and Chukanov, N.V. (2004) Crystal structure of the Na-, Ca-, Be-cordierite and crystallochemical regularities in the cordierite-sekaninaite series. Crystallography Reports, 49, 953–963.

Manuscript received March 15, 2011
Manuscript accepted June 7, 2011
Manuscript handled by G. Diego Gatta